Özgür Verim

https://doi.org/10.21278/TOF.461029121
ISSN 1333-1124
eISSN 1849-1391

DEVELOPMENT AND INVESTIGATION OF THE MECHANICAL BEHAVIOUR OF CIRCULAR EXTERNAL FIXATORS DURING THE GAIT CYCLE

Summary

In a study based on a tibia bone fractured in the diaphyseal region, a Circular External Fixator (CEF) was implanted in this region and its effects were investigated during gait. The CEF mounted on the adult human tibial fracture line is constructed from four standard rings. The six most effective states were selected in terms of force and moment values on the tibia during the human gait cycle. According to the results, it was determined that the stresses are at a maximum in the Kirschner wires in the lower segment. Hence, it was ascertained that the wire and bone junction regions are important and that the geometric and mechanical properties of the wires close to the fracture line should be improved.

Key words: bone fracture, circular external fixator, tibia, finite element analysis

1. Introduction

External fixators are systems that provide the stabilization of damaged limbs, the correction of skeletal deformities, the treatment of bone and joint injuries, and the elongation and alignment of bone limbs. A wide range of external fixator systems are available for surgical applications [1-3]. It has been observed that since each external fixator has its own morphological structure and mechanical characteristics, its stability and rigidity are different [1,4,5]. Considering all existing external fixator systems, CEF systems are the most important among them.

The CEF system is a modular system that can be easily modified before, during, and after the operation. A simple CEF system for osteosynthesis consists of parts such as rings, Kirschner wires, Schanz screws, connecting rods, wire holders, hinges, screws, and nuts. In CEF systems created by a certain hierarchical combination of these components, there are many factors that affect the biomechanical characteristics of the system. Some of these factors are the ring diameter, the material composition of the ring, the configuration of the ring structure, the number of wires, and the wire angle, wire diameter, wire pretension, and wire type [6-9].

In finite element studies performed on lower extremity fixator pairs, a point of the stance phase of the gait cycle is generally taken into consideration [10,11]. In fact, the variable loading type occurs as the reaction force on the bones in the gait cycle (stance phase–swing phase) [12-14]. In addition, finite element studies conducted on bone fixator pairs often take into account

certain muscle forces that are effective as boundary conditions [15-18]. Although the differences in boundary conditions are not considered in comparative studies, they are important in studies related to the strength of the part. Boundary conditions on the bone are obtained from software such as the AnyBody Modeling System (AMS) as well as experimental studies [14,19-21]. A lack of knowledge about which Kirschner wires are more important than others in a standard CEF system and which should be strengthened based on this information appears to be a deficiency in terms of understanding the CEF system. In this context, the main purpose of this study was to determine the stress distributions on Kirschner wires in a standard CEF system and to find out which are more meaningful for the system. In this study, the gait cycle created by the AMS software was divided into six parts according to the maximum reaction force and resultant moment values on the tibia bone. The mechanical characteristics of the parts in the CEF–tibia bone pair were examined according to the boundary conditions in each case.

2. Materials and methods

2.1 Use of the musculoskeletal model

The muscles and reaction force values of the tibial limb on the lower extremity of the human body used in the study were estimated by means of AMS software. This software can predict muscle and joint forces using the inverse dynamic method which is based on an analysis of kinematically indeterminate systems that use optimization methods [22,23]. The system, used to estimate how measurable motion states can be performed with defined mechanical systems, is used particularly in the fields of biomechanics, ergonomics, and orthopaedics [24]. For gait analysis in this study, the MOCAP-Driven Gait Models file in AnyBody software was simulated considering a complete cycle of the normal gait. The human model in the file takes into account the normal gait of a person with a mass of ~62 kg and a height of 162 cm.

2.2 Mounting of the CEF apparatus on the tibia bone

The standard CEF apparatus used for the treatment of the transverse fracture line formed in the diaphyseal region of the tibia bone consists of four rings and eight Kirschner wires. In the literature, ring diameters range from 150 to 180 mm [25-29]. In our study, the ring diameter used was 160 mm. Each ring was fixed on the tibia bone with stainless steel Kirschner wires of 1.8 mm diameter and 160 mm length. Two Kirschner wires were used to fix each ring. The CEF system was mounted on the tibia with the help of 8 Kirschner wires in total. The Kirschner wires on each ring were mounted onto the ring so that they were at a 90° angle to each other (Fig. 1).

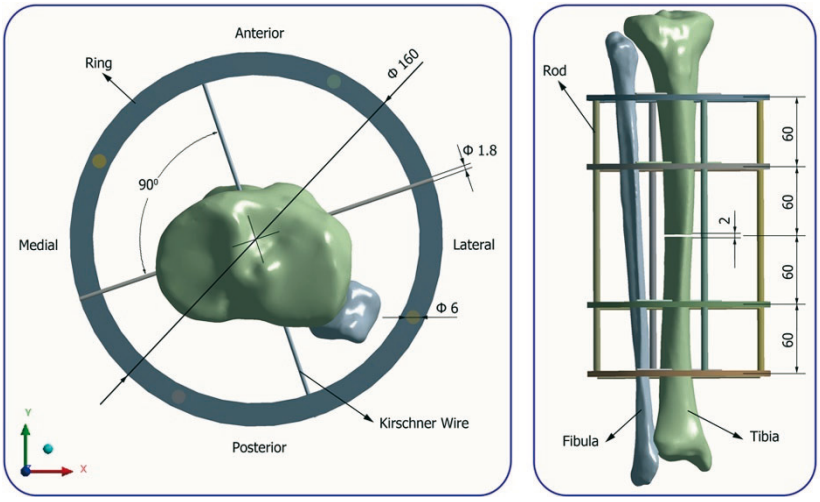

Fig. 1 Mounting and geometric measurements of parts on CEF apparatus on Tibia

A defect with a 2 mm gap occurred transversally in the tibial diaphyseal region [28]. The distance between the rings close to the fracture site and the distance between the two rings in the same direction were taken as 60 mm.

2.3 Muscle forces and boundary conditions applied to the finite element model

During the gait analysis, the right stance phase (60%), right swing phase (40%), and left stance phase (10%) were taken into account (Fig. 2a). Gait analysis within AnyBody software corresponds to 110% of a full cycle and 196 steps. During the analysis, when the reaction forces and moments arising from the body's centre of gravity and acting on the proximal tibia were examined, elevations were observed at certain points shown in Fig. 2c. These elevations were designated as steps 12, 59, 64, 76, 123, and 180 (Fig. 2b).

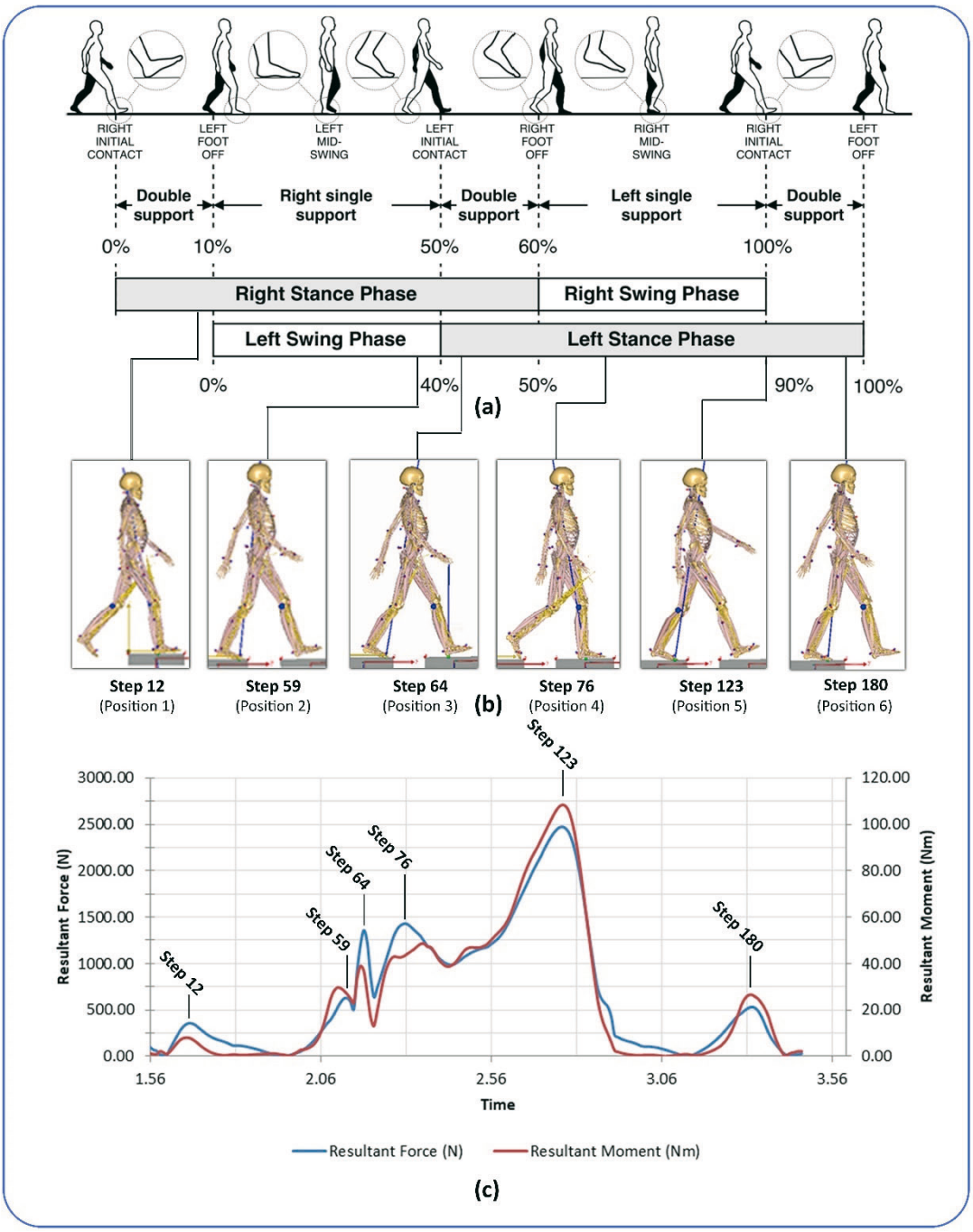

Fig. 2 The Phases of human gait analysis (a, b), resultant force and moment values acting on the knee cap (c)

In order to simplify the finite element model, inertial effects were ignored, and static analyses of the system were carried out. Considering a full cycle of the normal human gait, the finite element analysis was performed for six important points of the kneecap reaction forces (Fig. 2). The resultant reaction force and moment values on the left kneecap (Fig. 2b) were investigated separately and were converted into graphs (Fig. 2c).

In the gait analysis, the force values of the active muscles were determined in detail for each position (Fig. 3). The most active muscle groups were the soleus medialis (×3), soleus lateralis (×3), and rectus femoris (×2) in position 5 (step 123).

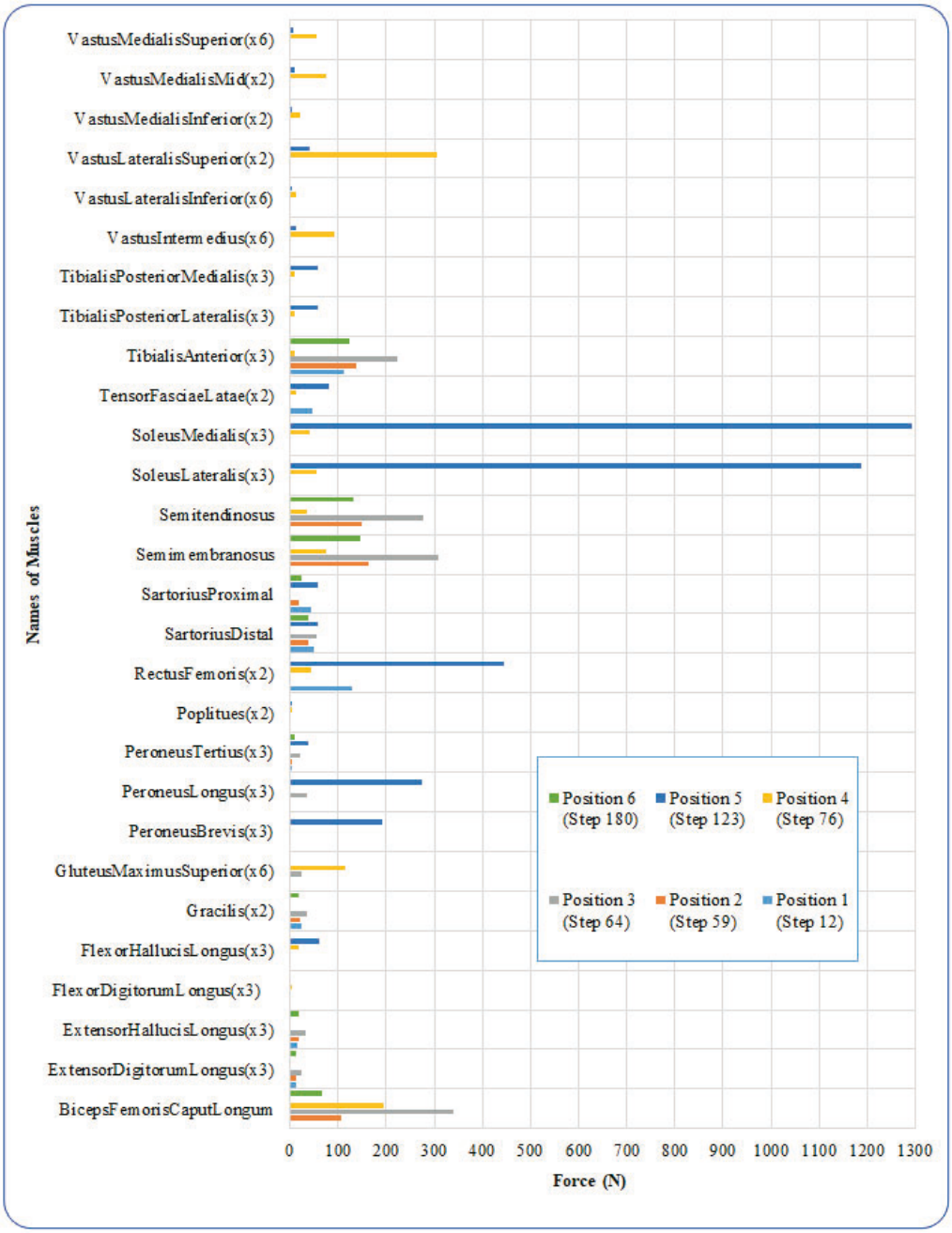

Fig. 3 Activity values of the muscles at the determined step values

This position (position 5) is seen as the last phase of the gait analysis, and in this case, the heel region of the foot is up and the toes touch the ground. Groups of many muscles are active and passive at different points in the gait analysis (196 steps). The activity and passivity values of the muscle groups according to the six selected positions are shown in Fig. 3.

2.4 Three-dimensional modelling and finite element analysis of a CEF–tibia bone pair

For three-dimensional modelling of the tibia bone, computed tomography images of the bone were first processed in Mimics software (Materialise, Belgium), and STL (Stereolithography) data of the cortical, trabecular, and marrow regions of the bone were obtained. The data were then transformed into a three-dimensional model with the surface form of NURBS (non-uniform rational B-spline) [30] using Geomagic Design X (3D Systems) reverse engineering software. A fracture was created on the tibia bone using SolidWorks 2018 (Dassault Systèmes) parametric modelling software and then the CEF apparatus was mounted on the tibia bone. The design was transferred to Ansys Workbench 18.2 finite element software (Ansys Inc.) where strength analysis of the CEF–tibia bone system was performed under the physical boundary conditions obtained from the AMS software (Fig. 4).

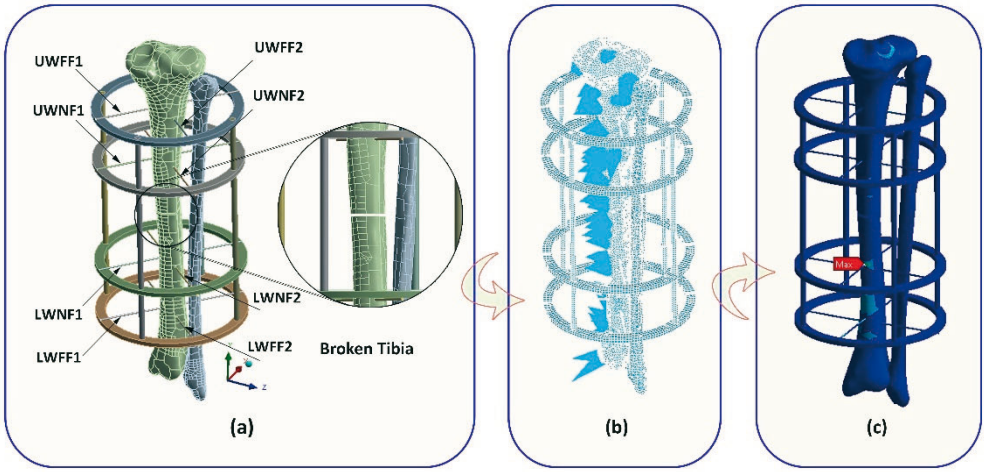

Fig. 4 Location of the CEF apparatus on the tibia and abbreviations of the names of Kirschner wire (a) Physical boundary conditions of the tibia obtained from AMS software (b) Equivalent von Mises stresses in the CEF-tibia system (c)

In the context of this study, bones and CEF apparatus were accepted as isotropic, linear elastic, and homogeneous. The mesh model of the CEF–tibia bone system consists of a total of 393,695 nodes and 195,468 elements. The tibia and fibula bone models consist of tetrahedral elements, while rings, Kirschner wires, and vertical bar holding rings together consist of hexahedral elements. The contact relationship in the Kirschner wire–ring and Kirschner wire–tibia bone connections was defined as “no separation contact”. The contact relationships of all other parts were determined as “bonded contact”. Since the general structure of the study was based on a comparative analysis, a linear solution method was chosen for the analysis. Material types and characterization of the parts in the CEF–tibia bone system are shown in Table 1.

Table 1 Mechanical characterization of parts in the IEF-tibia system

Part	Material	Tensile Strength (MPa)	Young Modulus (GPa)	Poisson Rate	Literature
Cortical	--	200 (Comp.)	17	0.3	[31, 32]
Trabecular	--	9.86	0.7	0.3	[33]
Marrow	--	--	0.3	0.45	[11]
Fibula	--	--	5	0.3	[32]
Ring	Stainless Steel	700	200	0.3	[6]
Rod	Stainless Steel	700	200	0.3	[6]
Kirschner Wire	Stainless Steel	700	200	0.3	[6]

The measured force and moment values that affect the kneecap joint during normal gait are presented in Fig. 5a-5b. These values were obtained from the AMS software using reverse dynamic analysis. The values were expressed in terms of spatial environment and body weight (BW). Force and moment values are given proportionally to body weight. Force values are given as BW and moment values as BW.m. The coordinates of the force and moment on the tibia bone are shown in Fig. 5c. When the muscular and joint forces are considered, the right and left tibial limbs exhibit symmetrical behaviour.

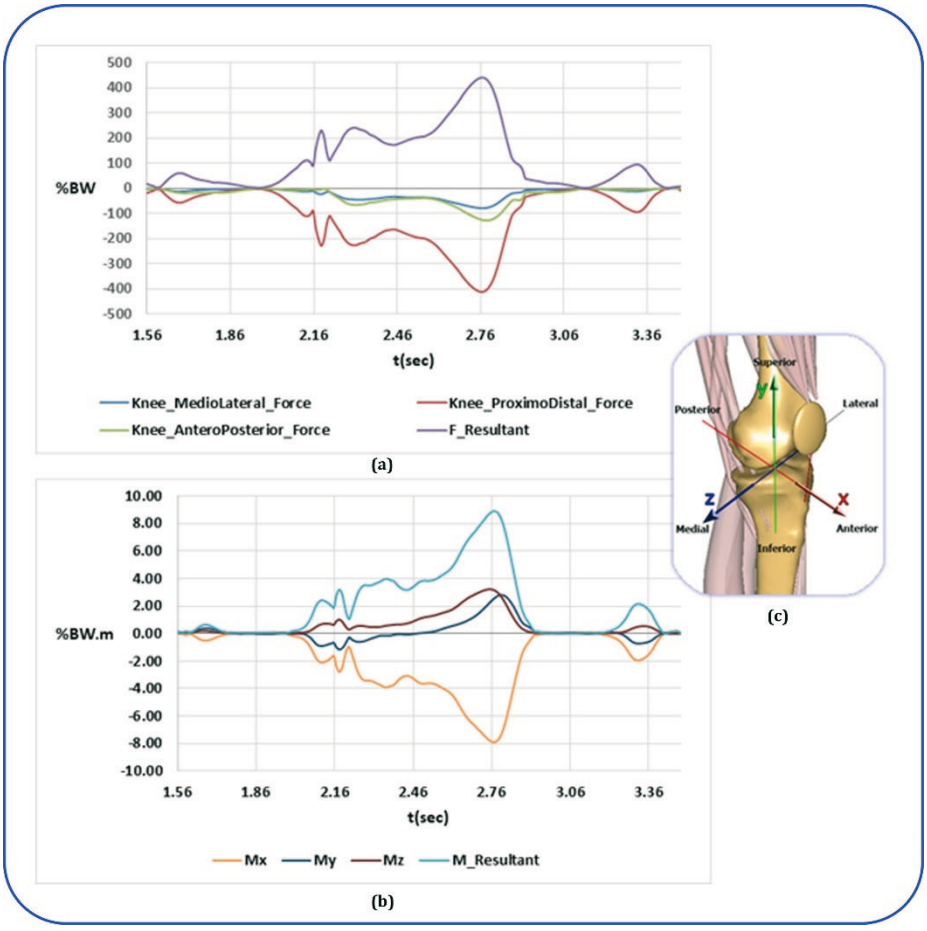

Fig. 5 Knee joint forces and moments on the tibia plateau during normal gait analysis

3. Results and discussion

According to the results of the finite element analysis of the six positions considered important during normal gait analysis of the tibia bone under the given boundary conditions, the maximum von Mises equivalent stress values were generally formed at the junction of the Kirschner wire and cortical bone (Fig. 6) [6].

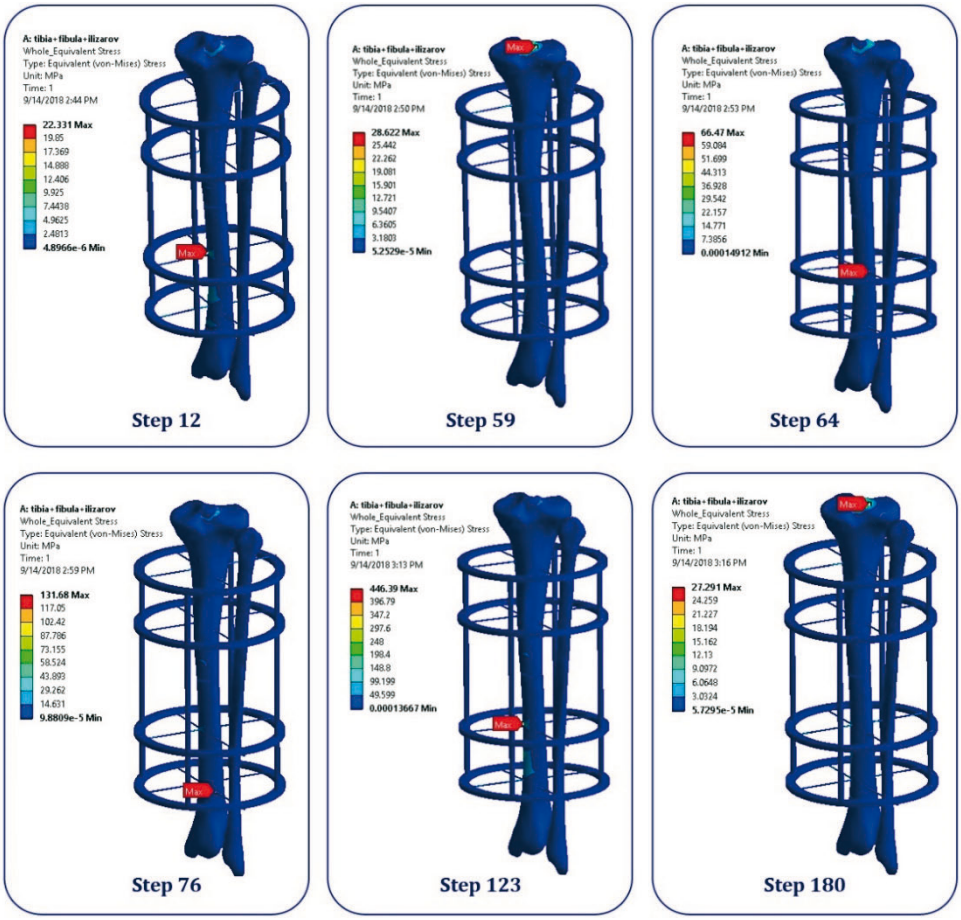

Fig. 6 The maximum von Mises equivalent stress values in the CEF-tibia system at specified step values

When the finite element analysis was examined, it was observed that the maximum von Mises equivalent stress values were, listed from highest to lowest, at step 123 (446.39 MPa), step 76 (131.68 MPa), step 64 (66.47 MPa), step 59 (28.62 MPa), step 180 (27.29 MPa), and step 12 (22.33 MPa), respectively. The stress values shown in Fig. 6 are approximately proportional to the resultant force and moment values that correspond to the step values determined in Fig. 2c. It was found that the stress values of the wires in the CEF–tibia bone system were more important than those of the other parts. In Table 2 and Fig. 4a, all wires in the CEF–tibia bone system are named according to their position (e.g., LWNF1 – lower wire near fracture 1, UWFF2 – upper wire far from fracture 2).

Table 2 The maximum von Mises equivalent stress values of wires in the CEF-tibia system (MPa)

Name of Wire	Step 12	Step 59	Step 64	Step 76	Step 123	Step 180
UWFF1	11.2	7.59	15.3	37.64	230.7	6.92
UWFF2	13	18.8	51.2	117	263.1	19.9
UWNF1	4.8	6.21	15.3	20.12	88.9	6.02
UWNF2	7.89	9.18	25.6	69.19	161.4	9.94
LWNF1	14	11.6	26.3	24.97	281.5	10.5
LWNF2	8.42	24.23	66.47	97.04	135.69	24.7
LWFF1	9.48	7.71	19.06	17.72	183.39	7.29
LWFF2	13.77	24.01	64.49	131.68	281.18	2.5

As shown in Table 2, the maximum stress values on the wires occurred in step 123. It was found that the stress values of the wires that had 2 at the end of their names were generally

higher than those of the wires that had 1 at the end of their names. Considering the stress values at each step of the wires, it was found that the most important wires were LWFF2 and UWFF2. The wire with the lowest stress values was UWNF1.

As a result of the study, it was observed that the maximum von Mises equivalent stress occurred at the junction of the bone and wires (Figs. 4 and 6) [6]. In this case, it was seen that the bone and Kirschner wires were under intense stress. However, stress values at the junction of the wire and bone did not reach the level of stress that would damage the cortical bone [10, 31, 32]. Donaldson et al. [10] examined the factors affecting loosening between the bone and wire in circular external fixators. In their studies, they observed that stress concentrations occurred in areas where the wire and bone joined the periosteum and endosteum. Mitousoudis et al. [6] reported a study on the biomechanical analysis of CEF. They observed that the maximum stress values occurred at the junction of the wire and bone. In addition, they saw that the stress values decreased as one goes to the middle parts of the wire. As different boundary conditions affected the CEF–tibia bone system in each gait phase, it was observed that the regions where the stress values were concentrated at each position were different (Fig. 6). In some steps where the boundary conditions are intense, the high stress values can be related to both the resultant force and moment values in the knee joint and the optimization of the mesh structure of the CEF–tibia bone system. Diffo Kaze et al. [12] examined the muscle forces and bone structures of the human lower extremity in detail, aiming to model the numerical analysis of implants placed in the human body more accurately. The main skeleton of our study overlaps with this study. With the gains obtained from our study, numerical studies of internal and external fixators suitable for every purpose added to the human body can be performed.

The sudden rising stress values occurring in steps 59, 123, and 180 are due to the irregular mesh structures at those points. The stress distributions in other regions were found to be at expected and normal levels (Fig. 6). Detailed mesh optimization of the CEF–tibia bone system can be performed in future studies due to the complexity of the bone structure [33]. Based on the stress values occurring in the CEF–tibia bone system, some improvements can be made to the CEF apparatus. In this context, the geometric and mechanical properties of the Kirschner wires in which the stress values are important in each phase state can be improved. In addition, the standard CEF apparatus can be arranged as a patient-specific hybrid apparatus [34].

The reason for the high resultant force and moment values occurring in step 123 is that the rectus femoris, peroneus longus, peroneus brevis, and most importantly the soleus lateralis and soleus medialis muscle groups are most active. The soleus lateralis and soleus medialis control the forward rotation of the tibia bone on the talus. If the soleus muscle group is weak, plantar flexion movement becomes difficult and the push phase of walking is impaired. When the study was examined in detail, it was found that the stress values of the wires that had 2 at the end of their names were generally higher than the stress values of the wires that had 1 at the end of their names (Table 2). Considering the muscle activities during gait, the reason for this is the higher efficiency values in the medial–lateral line than the activity values in the anterior–posterior line. The muscle groups on the tibia bone are concentrated in the posterior and lateral regions. The force and momentum values created by the line between the starting and ending points of the muscles can cause this effect.

4. Conclusions

When our study was evaluated in general, it was seen that gait phases were important in the general design of internal and external fixators, and it was revealed that analyses should be made according to these phases. In addition, according to the results of the study, it was determined that the wire and bone junction regions are important and that the geometric and mechanical properties of the wires close to the fracture line should be improved. In the future, CEF systems with the desired mechanical and geometric properties specific to the regions can

be designed by taking into account the stress values on the wires. Based on this, internal and external fixator designs and analysis can be performed during all kinds of activities (sitting, getting up, cycling, bodybuilding, etc.) with the help of the gains obtained from this study.

Acknowledgment

I would like to thank Afyonkarahisar Health Sciences University for its contributions to the Department of Anatomy.

REFERENCES

[1] Solomin, L. The basic principles of external skeletal fixation using the Ilizarov device (Google eBook). *Springer* **2008**

[2] Abd Aziz, A. U.; Wahab, A. H. A.; Rahim, R. A. A.; Kadir, M. R. A.; Ramlee, M. H. A finite element study: Finding the best configuration between unilateral, hybrid, and ilizarov in terms of biomechanical point of view. *Injury* **2020**, 51(11), 2474-2478. https://doi.org/10.1016/j.injury.2020.08.001

[3] Kouassi, K. J. E.; Cartiaux, O.; Fonkoué, L.; Detrembleur, C.; Cornu, O. Biomechanical study of a low-cost external fixator for diaphyseal fractures of long bones. *Journal of Orthopaedic Surgery and Research* **2020**, 15(1), 1-8. https://doi.org/10.1186/s13018-020-01777-5

[4] Yilmaz. E.; Belhan, O.; Karakurt, L.; Arslan, N.; Serin, E. Mechanical performance of hybrid Ilizarov external fixator in comparison with Ilizarov circular external fixator. *Clinical Biomechanics* **2003**, 18(6), 518–522. https://doi.org/10.1016/S0268-0033(03)00073-1

[5] Caja, V. L.; Kim, W.; Larsson, S.; Chao, E. Comparison of the mechanical performance of three types of external fixators: linear, circular and hybrid. *Clinical Biomechanics* **1995,** 10(8):401–406. https://doi.org/10.1016/0268-0033(95)00014-3

[6] Mitousoudis, A. S.; Magnissalis, E. A.; Kourkoulis, S. K. A biomechanical analysis of the Ilizarov external fixator. *EPJ Web of Conferences* **2010,** 95-105. https://doi.org/10.1051/epjconf/20100621002

[7] Lewis, D. D.; Bronson, D. G.; Samchukov, M. L.; Welch, R. D.; Stallings, J. T. Biomechanics of circular external skeletal fixation. *Veterinary Surgery* **1998**, 27(5):454–464. https://doi.org/10.1111/j.1532-950X.1998.tb00156.x

[8] Kumar, D. B.; Vijayakumar, K.; Martin, A. V.; George, R. Review of biomechanical characteristics of Illizarov ring fixators using FEA. In IOP Conference Series: Materials Science and Engineering **2020**, 993, 1, 012037. https://doi.org/10.1088/1757-899X/993/1/012037

[9] Ganadhiepan, G.; Zhang, L.; Miramini, S.; Mendis, P.; Patel, M.; Ebeling, P.; Wang, Y. The effects of dynamic loading on bone fracture healing under Ilizarov circular fixators. *Journal of Biomechanical Engineering* **2019**, 141(5). https://doi.org/10.1115/1.4043037

[10] Donaldson, F. E.; Pankaj, P.; Simpson, A. H. R. W. Investigation of factors affecting loosening of ilizarov ring-wire external fixator systems at the bone-wire interface. *Journal of Orthopaedic Research* **2012***,* 30(5):726–732. https://doi.org/10.1002/jor.21587

[11] Tarapoom, W.; Puttapitukporn, T. Stress distribution in human tibia bones using finite element analysis. *Engineering Journal* **2016***,* 20(3):155–167. https://doi.org/10.4186/ej.2016.20.3.155

[12] Diffo Kaze, A.; Maas, S.; Arnoux, P. J.; Wolf, C.; Pape, D. A. Finite element model of the lower limb during stance phase of gait cycle including the muscle forces. *BioMedical Engineering OnLine* **2017***,* 16(1):138. https://doi.org/10.1186/s12938-017-0428-6

[13] Seo, J. W.; Kang, D. W.; Kim, J. Y.; Yang, S. T.; Kim, D. H.; Choi, J. S.; Tack, G. R. Finite element analysis of the femur during stance phase of gait based on musculoskeletal model simulation. *Bio-Medical Materials and Engineering* **2014***,* 24(6), 2485–2493. https://doi.org/10.3233/BME-141062

[14] Ricci, P. L.; Maas, S.; Kelm, J.; Gerich, T. Finite element analysis of the pelvis including gait muscle forces: an investigation into the effect of rami fractures on load transmission. *Journal of Experimental Orthopaedics* **2018***,* 5(1), 33. https://doi.org/10.1186/s40634-018-0151-7

[15] Koh, Y. G.; Son, J.; Kim, H. J.; Kwon, S. K.; Kwon, O. R.; Kim, H. J.; Kang, K. T. Multi-objective design optimization of high tibial osteotomy for improvement of biomechanical effect by using finite element analysis. *Journal of Orthopaedic Research* **2018***,* 36(11), 2956–2965. https://doi.org/10.1002/jor.24072

[16] Pauchard, Y.; Ivanov, T. G.; McErlain, D. D.; Milner, J. S.; Giffin, J. R.; Birmingham, T. B.; Holdsworth, D. W. Assessing the local mechanical environment in medial opening wedge high tibial osteotomy using finite element analysis. *Journal of Biomechanical Engineering* **2015***,* 137(3), 31005. https://doi.org/10.1115/1.4028966

[17] Golovakha, M. L.; Orljanski, W.; Benedetto, K. P.; Panchenko, S.; Büchler, P.; Henle, P.; Aghayev, E. Comparison of theoretical fixation stability of three devices employed in medial opening wedge high tibial osteotomy: A finite element analysis. *BMC Musculoskeletal Disorders* **2014**, 15(1), 230. https://doi.org/10.1186/1471-2474-15-230

[18] Chen, F.; Huang, X.; Ya, Y.; Ma, F.; Qian, Z.; Shi, J.; Guo, S.; Yu, B. Finite element analysis of intramedullary nailing and double locking plate for treating extra-articular proximal tibial fractures. *Journal of Orthopaedic Surgery and Research* **2018**, 13(1), 12. https://doi.org/10.1186/s13018-017-0707-8

[19] Grujicic, A.; Laberge, M.; Xie, X.; Arakere, G.; Pandurangan, B.; Grujicic, M.; Jeray, K. J.; Tanner, S. L. Computational investigation of the relative efficacies of nail- and plate-type proximal femoral-fracture fixation implants. *Multidiscipline Modeling in Materials and Structures* **2011**, 7(3), 212–244. https://doi.org/10.1108/1536-540911178234

[20] Grujicic, M.; Xie, X.; Arakere, G.; Grujicic, A.; Wagner, D. W.; Vallejo, A. Design-optimization and material selection for a proximal radius fracture-fixation implant. *Journal of Materials Engineering and Performance* **2010**, 19(8), 1090–1103. https://doi.org/10.1007/s11665-009-9591-7

[21] Mehle, K.; Eckert, A.; Gentzsch, D.; Schwan, S.; Ludtka, C.; Knoll, W. Evaluation of a new PEEK mandibular reconstruction plate design for continuity defect therapy by finite element analysis. *International Journal of New Technology and Research 2016,* 2(7), 263461.

[22] Erdemir, A.; McLean, S.; Herzog, W.; Van Den Bogert, A. J. Model-based estimation of muscle forces exerted during movements. *Clinical Biomechanics* **2007**, 22(2), 131–154. https://doi.org/10.1016/j.clinbiomech.2006.09.005

[23] Damsgaard, M.; Rasmussen, J.; Christensen, S. T.; Surma, E.; De Zee, M. Analysis of musculoskeletal systems in the AnyBody Modeling System. *Simulation Modelling Practice and Theory* **2006**, 14(8), 1100–1111. https://doi.org/10.1016/j.simpat.2006.09.001

[24] Rasmussen, J.; Damsgaard, M.; Christensen, S. T. Inverse-inverse dynamics simulation of musculo-skeletal systems. *Royal Acedemy of Medicine in Ireland* **2000**.

[25] Kourkoulis, S. K.; Mitousoudis, A. An experimentally validated model for the ilizarov fixator considering the loss of wire's pretension. *Engineering Transactions* **2016**, 64(4), 621–627.

[26] Huang, Y.; Zhang, C.; Luo, Y. A comparative biomechanical study of proximal femoral nail (InterTAN) and proximal femoral nail antirotation for intertrochanteric fractures. *International Orthopaedics* **2013**, 37(12), 2465–2473. https://doi.org/10.1007/s00264-013-2120-1

[27] Zhang, G. Geometric and material nonlinearity in tensioned wires of an external fixator. *Clinical Biomechanics* **2004**, 19(5), 513–518. https://doi.org/10.1016/j.clinbiomech.2004.01.009

[28] Gessmann, J.; Jettkant, B.; Schildhauer, T. A.; Seybold, D. Mechanical stress on tensioned wires at direct and indirect loading: A biomechanical study on the Ilizarov external fixator. *Injury* **2011**, 42(10), 1107–1111. https://doi.org/10.1016/j.injury.2011.02.001

[29] Yang, L.; Nayagam, S.; Saleh, M. Stiffness characteristics and inter-fragmentary displacements with different hybrid external fixators. *Clinical Biomechanics* **2003**, 18(2), 166–172. https://doi.org/10.1016/s0268-0033(02)00175-4

[30] Milić, P.; Marinković, D. Isogeometric FE analysis of complex thin-walled structures. *Transactions of FAMENA* **2015**, 39(1), 15-26.

[31] Kemper, A. R.; McNally, C.; Kennedy, E. A.; Rath, A. L.; Manoogian, S. J.; Stitzel, J. D.; Duma, S. M.; Matsuoka, F.; Hasegawa, J. Methods for dynamic material testing of human cortical bone specimens. *The 32nd International Workshop on Human Subjects for Biomechanical Research* **2004**, 31(1952), 31–46.

[32] Moewis, P.; Checa, S.; Kutzner, I.; Hommel, H.; Duda, G. N. Physiological joint line total knee arthroplasty designs are especially sensitive to rotational placement – A finite element analysis. *PLoS One* **2018**, 13(2), e0192225. https://doi.org/10.1371/journal.pone.0192225

[33] Lobos, C.; Payan, Y.; Hitschfeld, N. Techniques for the generation of 3D finite element meshes of human organs. *Informatics in Oral Medicine: Advanced Techniques in Clinical and Diagnostic Technologies* **2010**, 126–158. https://doi.org/10.4018/978-1-60566-733-1

[34] Corona, P. S.; Vicente, M.; Tetsworth, K.; Glatt, V. Preliminary results using patient-specific 3d printed models to improve preoperative planning for correction of post-traumatic tibial deformities with circular frames. *Injury* **2018**, 49, 51–59. https://doi.org/10.1016/j.injury.2018.07.017

Submitted: 26.3.2021

Accepted: 10.01.2022

Özgür VERİM
ozgurverim@aku.edu.tr
Afyon Kocatepe University, Faculty of Technology, Department of Mechanical Engineering, 03200, Afyonkarahisar, Turkey